2003-01-1717

Effect of Welded or Glued Joints on Modal Properties of an Assembly

Pavak Mehta and Rajendra Singh
Center for Automotive Research, The Ohio State University

ABSTRACT

This paper examines the natural frequencies, mode shapes and modal damping ratios of a specially designed laboratory fixture with integral, welded or glued joints. The influence of these alternate joints on the dynamic properties of an assembly is demonstrated, using experimental, computational and analytical methods. Dimensions of a typical welded joint configuration are varied to study their effects on the modal properties of an assembly. Predictions are successfully compared with experimental modal data. This study should help in selecting the welded joint configuration to meet strength, durability or dynamic design criteria.

INTRODUCTION

Static and dynamic behaviors of an assembled structure are significantly affected by its joints (bolted, welded, glued). Singh et. al. [1] have theoretically and experimentally shown the effect of welded, riveted and adhesive joints on the natural frequencies of generic 'L', "T", and "U" sheet metal structures. Technologies such as space frames and hydroforming facilitate ground vehicles with both lighter and stiffer frame members. However, the welds or adhesives used to join the members may contribute up to half of an assembly's dynamic compliance and most of its damping [2,3]. To quantify such effects, it is obviously desirable to develop accurate dynamic models of a frame [3]. Overall, the role of joints in the static stiffness, natural frequencies, mode shapes and damping determining of assemblies must be clearly understood.

PROBLEM FORMULATION

The fixture used for analytical and experimental studies is composed of two rigid steel blocks connected by an elastic joint as shown in Figure 1. Specifically, the joint is viewed as a combination of an elastic beam and two end interfaces at points 2 and 3 where integral, welded or glued joints exist. The scope of this work is limited to the first two vibration modes of an assembly having motions in the x-y plane though all relevant modes are measured and computed as a part of our work.

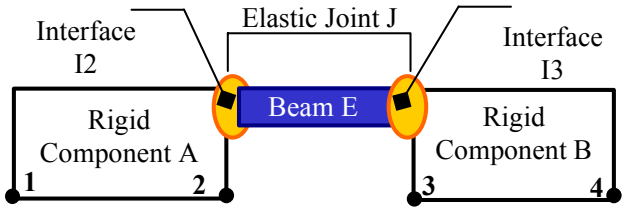

Figure 1. Joined assembly where the elastic joint is shown as a combination of elastic beam and interfaces.

Key examples with alternate joints are listed in Table 1. Based upon the elastic beam configuration used by Young et. al. [4], finite element models are created for modal analysis and they are grouped under Example C. Case C0 of Figure 2 is an integral (or ideal) joint case and cases C1 through C8 consider joints with different weld configurations as shown in Figure 3. In cases C1 to C8, the elastic beam is welded to rigid blocks via different weld zones. The weld makes 45° angels with x and z coordinates. Weld zones along the width of the beam are referred to as zone-I and four different zones along the length are labeled as zone-II (Figure 3c-d and Table 2). The weld thickness h_w is held constant in both zones. In C7 and C8, the weld is applied along the length of beam, i.e. only in zone-I with a recess in between. To ensure that only the welded connections exist at the interface that is between the beam and end blocks, a gap of 1 mm size is created in models. Figure 4 schematically shows integral joint examples (D0, E0, F01 and F02). Case DO is created to compare the welded interface from cases E1 to E5, and cases F01 and F02 are compared with glued interface cases F1 and F2 respectively. Case E0 is an analytical or finite element model that is used to compare experimental results of

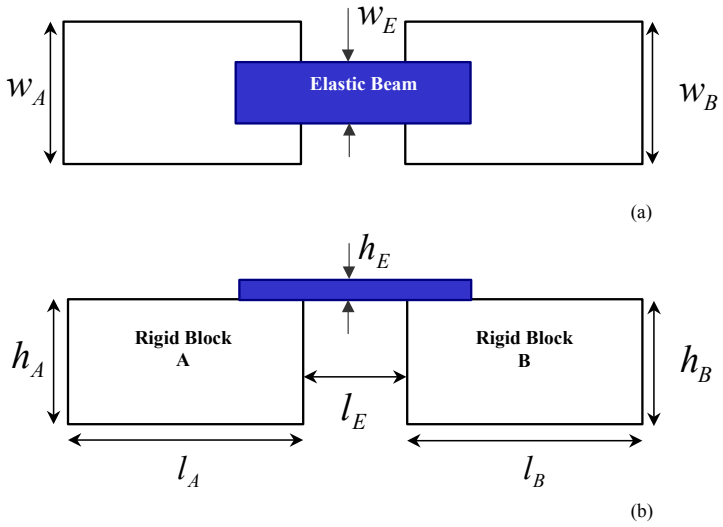

Figure 2. Dimensions of integral case C0. (a) Plan. (b) Elevation.

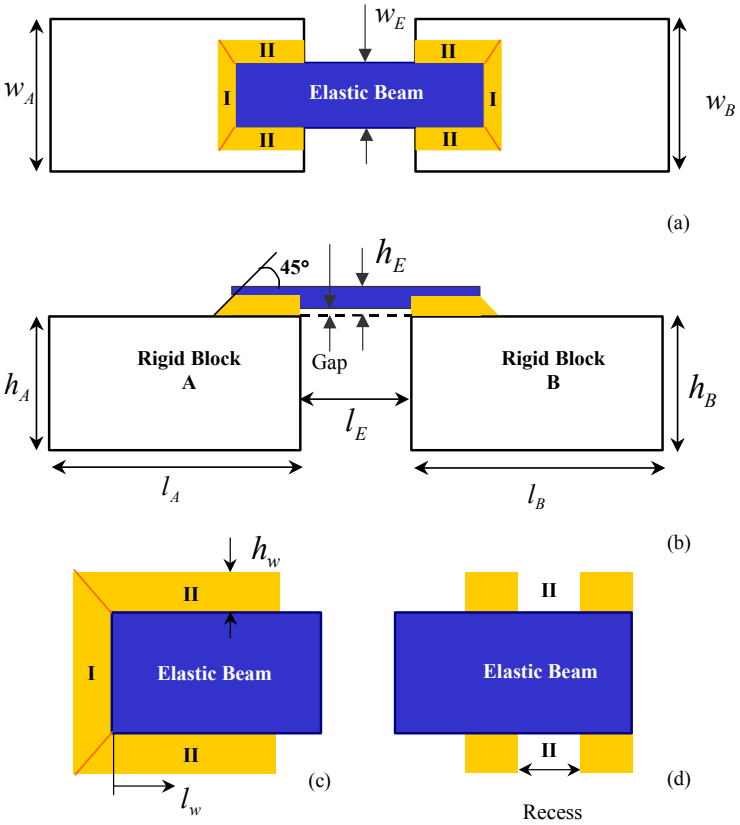

Figure 3. Schematics of welded cases C1 to C8. (a) Plan. (b) Elevation. (c) Magnified plan of weld interface between the elastic beam and rigid block for cases C1 to C6. (d) Plan of weld configurations for cases C7 and C8.

cases E1 through E5 as described in Table 3. Like Example C, a gap of 0.1 mm size is kept between the elastic beam and rigid blocks in Example E. To begin with, in case E1 the beam corners are tack welded to the block while in rest of the four cases, the beam is fillet welded to blocks along the width (in z direction). In cases E2 and E3 it is only in the center but in cases E4 and E5 the entire edge is welded (Table 3). Only the upper edge is welded in cases E2 and E4 while in cases E3 and E5 both edges of the beam are welded to rigid blocks. The geometric dimensions of the blocks and beams for cases E1 to E5 are slightly different from each other and also from case D0 due to the fabrication problems. Nominal dimensions along with tolerances are calculated for all five cases, and then only the nominal values are used for analytical as well as finite element models (Table 1). Example F consists of four cases, F01, F02, F1 and F2 where F01 and F02 are integral joint models for cases F1 and F2 respectively (Figure 4). A thick steel beam is glued to rigid blocks using silicone glue in case F1 (Figure 5a). Case F2 considers a thin steel beam glued to two rigid blocks using steel filler (Figure 5b).

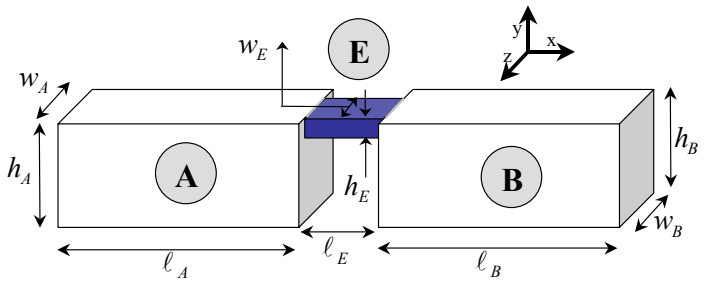

Figure 4. Schematic for integral cases (D0, E0, F01 and F02) of Table 1. Key: A=Rigid block A; B=Rigid block B; E=Elastic Beam h=Thickness; ℓ=Length; w=Width; x, y, z=Cartesian coordinates.

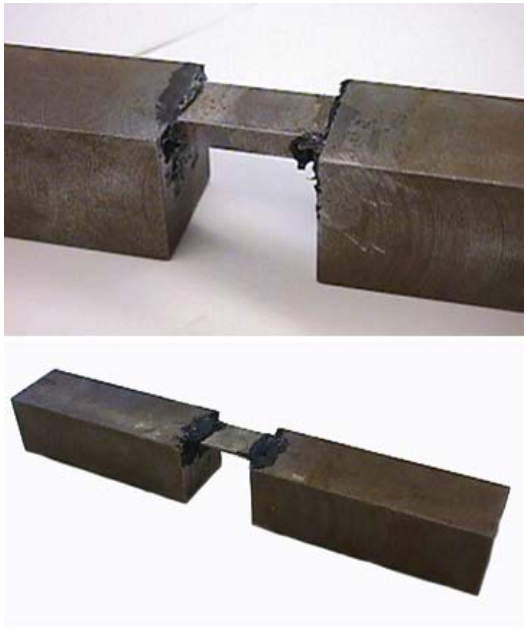

Figure 5. Photographs of Example F. (a) Case F1. (b) Case F2.

Example	Case	Joint or Interface	Dimensions (ℓ, w, h) in mm			Method		
			Blocks	Beam		EXP	FEM	SIM
Example C	C0	Integral	$\ell_{A,B} = 75$ $w_{A,B} = 25$ $h_{A,B} = 25$	$\ell_E = 13$ $w_E = 13$ $h_E = 4.8$			✔	✔
	C1	Welded					✔	
	C2						✔	
	C3						✔	
	C4						✔	
	C5						✔	
	C6						✔	
	C7						✔	
	C8						✔	
Example D	D0	Integral	$\ell_{A,B} = 127.2$ $w_{A,B} = 50.7$ $h_{A,B} = 50.7$	$\ell_E = 76.0$ $w_E = 25.3$ $h_E = 6.4$		✔	✔	✔
Example E	E0	Integral	$\ell_{A,B} = 127.2$ $w_{A,B} = 50.9$ $h_{A,B} = 50.7$	$\ell_E = 76.2$ $w_E = 24.9$ $h_E = 6.5$			✔	✔
	E1	Welded				✔	✔	
	E2					✔	✔	
	E3					✔	✔	
	E4					✔	✔	
	E5					✔	✔	
Example F	F01	Integral	$\ell_{A,B} = 75$ $w_{A,B} = 25$ $h_{A,B} = 25$	$\ell_E = 25$ $w_E = 13$	$h_E = 4.8$	✔	✔	✔
	F02				$h_E = 1.2$	✔	✔	✔
	F1	Glued (Epoxy)			$h_E = 4.8$	✔		
	F2				$h_E = 1.2$	✔		

Table 1. List of examples studied. Refer to Figure 1 for interfaces I2 and I3. Methodology Key: SIM=analytical, FEM=finite element, EXP=experimental.

Example C	**Weld zone-I, h_w = 3.4 mm**	**Weld zone-II, h_w = 3.4 mm**
Case C1	Entire zone-II	
Case C2		ℓ_w = 1 mm
Case C3		ℓ_w = 5 mm
Case C4		ℓ_w = 15 mm
Case C5		Entire zone-I
Case C6	Entire zones I and II	
Case C7		Recess = 11.5 mm
Case C8		Recess = 7.5 mm

Table 2. Description of weld configurations for cases C1-C8.

Example	Magnified sketch at the weld interface	Weld dimensions (mm)	
		Upper edge	Lower edge
E1	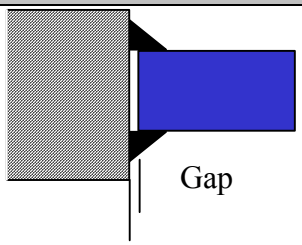	$\ell_w = 3.1$ $w_w = 3.1$ $h_w = 6.5$ Gap = 0.1	
E2	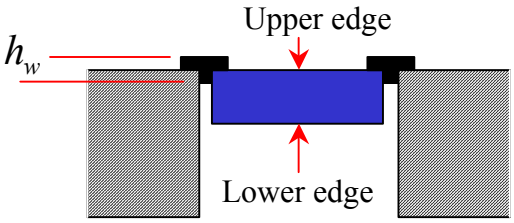	$\ell_w = 6.1$ $w_w = 15$ $h_w = 3$ Gap = 0.1	-
E3	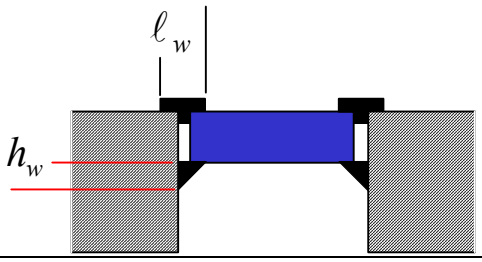	$\ell_w = 6.1$ $w_w = 15$ $h_w = 3$ Gap = 0.1	$\ell_w = 3.1$ $w_w = 15$ $h_w = 3.1$ Gap = 0.1
E4	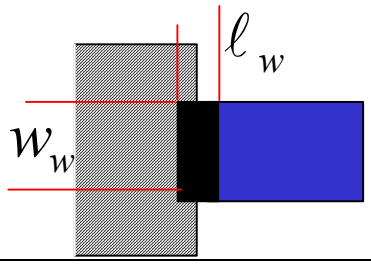	$\ell_w = 7.1$ $w_w = 24.9$ $h_w = 2.5$ Gap = 0.1	-
E5	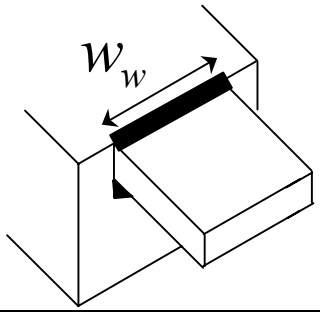	$\ell_w = 6.1$ $w_w = 24.9$ $h_w = 2.5$ Gap = 0.1	$\ell_w = 3.1$ $w_w = 24.9$ $h_w = 3.1$ Gap = 0.1

Table 3. Weld configurations and dimensions for Examples E1-E5.

Chief objective of this study is to determine and compare natural frequencies (ω_r), mode shapes (Φ_r), and damping ratios (ζ_r) of an assembly joined with alternate joints. In addition, we will develop and validate the analytical and computational models. Integral joint models (Examples C0, D0, E0, F01 and F02) are considered as ideal cases and hence their modal will serve as a baseline for comparison with properties of other joint examples.

FINITE ELEMENT METHOD (FEM)

FEM models were created for cases C0-C8, D0, E0-E5, F01 and F02. All FEM models were created using solid brick (20 nodes element) or/and solid tetrahedron (10 nodes element). Brick element has three degrees-of-freedom (DOFs) at each node, translation along x, y and z while tetrahedron element describes six DOFs at each node, three translational plus three rotational DOFs about the x, y and z-axes. Figure 6 shows the FEM model of Example D0, meshed with brick elements. Since limited the scope of our study, DOFs of each node are constrained such that assembly can translate about the y-axis and rotate about the z-axis. The interface or joint between the beam and rigid blocks is modeled with common nodes at the interfaces. Eigenvectors and eigenvalues for an undamped, unforced system are then obtained and studied. The animated display of mode shapes obtained using ANSYS [5] portrays a clear vision of the modal deflections of assembly.

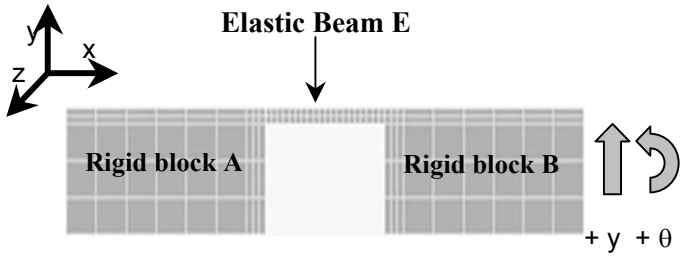

Figure 6. FEM model of example D0, meshed with solid brick

EXPERIMENTAL MODAL ANALYISIS (EXP)

Experimental modal analysis is important among the three methods as modal damping ratios (ζ_r), can be extracted in addition to natural frequencies (f_r) and mode shapes (Φ_r). In order to conduct experimental modal analysis, a dynamic force ($\tilde{F}(\omega)$) is applied to the structure and its transverse deflection ($\tilde{Y}(\omega)$) is measured, with measured frequency response functions (FRFs), system's natural frequencies, mode shapes and damping ratios can be extracted [6,7]. In our study, the LMS [8] software is used for that purpose. In the experimental setup, the assembly is freely suspended using bungee cords. Using piezoelectric force transducer (impulse hammer), assembly is excited by impacting at two distinct locations, though one at a time (Figure 7). We ensure that the excitation is symmetrical and in positive direction only. Acceleration ($\tilde{\ddot{Y}}(\omega)$) is then measured using uniaxial accelerometer given impulse excitations of magnitudes $\tilde{F}_1(\omega)$ and $\tilde{F}_2(\omega)$ at locations 1 and 2 respectively. Accelerometers are glued to the structure using superglue at locations 1, 2, 3 and 4 as shown in Figure 7. When excitation is applied at locations, four accelerations are simultaneously measured. Hence there are total eight (4×2) translational FRFs for each assembly. Measured FRFs from experiments are in accelerance form ($\tilde{\ddot{Y}}/F(\omega)$) type, which are then converted into dynamic compliance ($\tilde{Y}/F(\omega)$) FRFs using the LMS software by integrating the accelerance twice in the frequency domain. Simultaneous measurements of acceleration at four locations, for a single impact, gives accurate results and yet saves time. In order to avoid the aliasing effect, maximum frequency (f_{max}) is slightly more than twice the frequency range of interest. Frequency resolution (Δf) is 2.5 Hz and eight averages are used. Experiments are carried out for all physical structures, (Examples D0, E1-E5, F1, F2, F01 and F02). Typical measured FRFs are displayed in Figures 11,12 and 13.

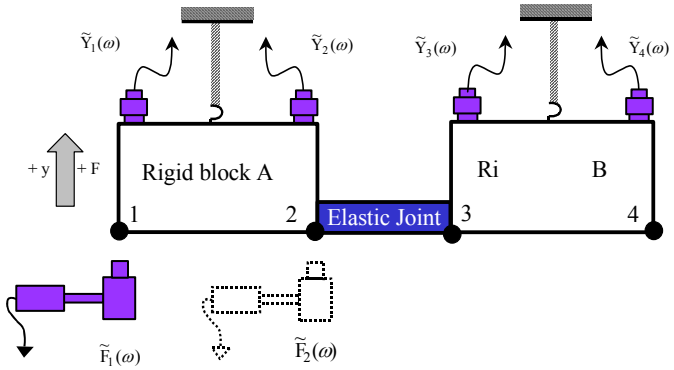

Figure 7. Experimental assembly along with locations of excitation and response.

ANALYTICAL SIMULATION (SIM)

In order to conduct analytical modal analysis, system mass matrix (**M**) and system stiffness matrix (**K**) are required. The goal is to mathematically model the physical structure to obtain natural frequencies (f_r) and mode shapes (Φ_r), which are then confirm by EXP and FEM results. Analytical modeling is only possible for integral joints as the dynamic properties of welded and glued (epoxy) joints are unknown. Hence, SIM models are created only for Examples D0, E0, F01 and F02. Assembly of Figure 8 consists of two rigid blocks (A and B) and an elastic beam (E). Blocks A and B are rigid bodies because their first flexural modes occur at 11 kHz, which is well beyond the frequency range of interest.

Here, each rigid body (A or B) has two DOFs, translation along the y-axis and rotation about the z-axis. Mass

matrices for rigid blocks A and B are derived with reference point at locations 2 and 3 respectively [4].

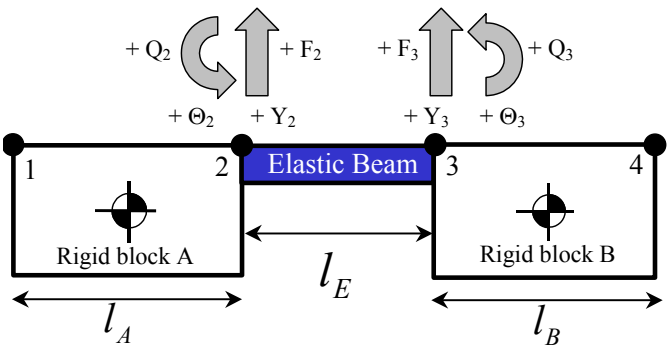

Figure 8. Schematic of example D0, described in terms of two rigid blocks (A and B) and an elastic beam (E).

Given the governing equations of motion for force and moment excitations at locations 2 and 3, individual mass matrices for block A and B are

$$\mathbf{M}_A = \begin{bmatrix} \mathrm{M}_A & -(\ell_A/2)\mathrm{M}_A \\ -(\ell_A/2)\mathrm{M}_A & \mathrm{J}_{A2} \end{bmatrix} \quad (1a)$$

$$\mathbf{M}_B = \begin{bmatrix} \mathrm{M}_B & (\ell_B/2)\mathrm{M}_B \\ (\ell_B/2)\mathrm{M}_B & \mathrm{J}_{B3} \end{bmatrix} \quad (1b)$$

To calculate the assembly mass matrix **M, $\mathbf{M}_B$** of block B is appended to **$\mathbf{M}_A$**, as shown below [4].

$$\mathbf{M} = \begin{bmatrix} \mathrm{M}_A & -\frac{\ell_A}{2}\mathrm{M}_A & 0 & 0 \\ -\frac{\ell_A}{2}\mathrm{M}_A & \mathrm{J}_{A2} & 0 & 0 \\ 0 & 0 & \mathrm{M}_B & \frac{\ell_B}{2}\mathrm{M}_B \\ 0 & 0 & \frac{\ell_B}{2}\mathrm{M}_B & \mathrm{J}_{B3} \end{bmatrix} \quad (2)$$

System mass matrix contains not only the diagonal terms but also the off-diagonal terms. Coupling in the mass matrix is referred to as the dynamic coupling, which is the case here. Assuming beam as a massless component, its theoretical stiffness can be derived using the Euler's beam theory as described by Thomson [9]. Positive sign convention for four distinct deflections at the end of a uniform beam are shown in Figure 8. Each element of stiffness matrix is related to the static deflection at the end taken separately, and the superposition of four deflections gives the static stiffness matrix associated with elastic beam (3) [4]. For instance, the first column of the stiffness matrix indicates force and moment required at locations 2 and 3 given arbitrary transverse deflection at location 2.

$$\begin{Bmatrix} \tilde{\mathrm{F}}_2 \\ \tilde{\mathrm{Q}}_2 \\ \tilde{\mathrm{F}}_3 \\ \tilde{\mathrm{Q}}_3 \end{Bmatrix} = \mathbf{K}_E^s \begin{Bmatrix} \tilde{\mathrm{Y}}_2 \\ \tilde{\Theta}_2 \\ \tilde{\mathrm{Y}}_3 \\ \tilde{\Theta}_3 \end{Bmatrix} \quad (3)$$

where,

$$\mathbf{K}_E^s = \begin{bmatrix} \mathbf{K}_a & \mathbf{K}_b \\ \mathbf{K}_c & \mathbf{K}_d \end{bmatrix} \quad (4a)$$

$$\mathbf{K}_a = \begin{bmatrix} \mathrm{K}_{FY} & \mathrm{K}_{F\theta} \\ \mathrm{K}_{QY} & \mathrm{K}_{Q\theta} \end{bmatrix} \quad (4b)$$

$$\mathbf{K}_b = \begin{bmatrix} -\mathbf{K}_{FY} & -\mathbf{K}_{F\theta} \\ (\mathbf{K}_{QY} - \ell_E \mathbf{K}_{FY}) & (-\mathbf{K}_{Q\theta} + \ell_E \mathbf{K}_{F\theta}) \end{bmatrix} \quad (4c)$$

$$\mathbf{K}_c = \begin{bmatrix} -\mathbf{K}_{FY} & -\mathbf{K}_{F\theta} \\ (-\mathbf{K}_{QY} + \ell_E \mathbf{K}_{FY}) & (-\mathbf{K}_{Q\theta} + \ell_E \mathbf{K}_{F\theta}) \end{bmatrix} \quad (4d)$$

$$\mathbf{K}_d = \begin{bmatrix} \mathrm{K}_{FY} & -\mathrm{K}_{F\theta} \\ -\mathrm{K}_{QY} & \mathrm{K}_{Q\theta} \end{bmatrix} \quad (4e)$$

$$\text{where } \mathrm{K}_{FY} = 12\mathrm{EI}/\ell_E{}^3;\ \mathrm{K}_{F\theta} = 6\mathrm{EI}/\ell_E{}^2;\ \mathrm{K}_{QY} = 6\mathrm{EI}/\ell_E{}^2;\ \text{and } \mathrm{K}_{Q\theta} = 4\mathrm{EI}/\ell_E \quad (5a\text{-}d)$$

Using the system matrices **M** and **K,** both of dimension 4 eigensolutions (λ_r) and eigenvectors (Φ_r) are obtained as follows:

$$\mathbf{K}\Phi_r = \lambda_r \mathbf{M}\Phi_r \quad (6)$$

Predictions of SIM model implemented using MATLAB [10], are then compared with the results of EXP and FEM models, as described in the following section.

MODES OF INTEREST

For all relevant examples, natural frequencies (f_r), mode shapes (Φ_r) and damping ratios (ζ_r) are obtained using FEM, EXP or SIM models. Table 4 summarizes modal properties in terms of models and examples.

Modal analysis of FEM models (without constraining any DOFs) gives all natural frequency and mode shapes of the assembly. First six system modes are obtained and studied (Figure 9) for Examples D0, E1-E5. The first mode (r = 1) of vibration (Figure 9a) shows rotation of both rigid blocks about the z-coordinate, where blocks A and B rotate in phase in x-y plane. This mode shape represents rotational stiffness elements of the joint (Figure 10a). The second mode (r = 2) of vibration (Figure 9b) illustrates a twisting motion of the assembly about the x-coordinate. Here, blocks A and B rotate out of phase and hence introduce a twist in the elastic joint (J). The third mode of vibration (r = 3) shows rotation of assembly about the y-coordinate, where blocks (A and B) rotate in phase (Figure 9c). In the fourth mode (r = 4), individual block rotates about the z-coordinate, which causes shear movement of the elastic joint connecting them (Figure 9d). This mode shape thus represents shear stiffness element of the elastic joint stiffness matrix (Figure 10b). The fifth mode (r = 5) of vibration is the out of phase rotation of individual blocks (A or B) about the y-coordinate. Notice, the edges connecting elastic beam (E) also deform, hence the blocks are no longer rigid (Figure 9e). Sixth mode (r = 6) of vibration is the displacement of two rigid blocks (A and B) along the x-coordinate with little rotation at the end of each block about the z-coordinate. Longitudinal displacement of blocks places the joint under compression and tension. Thus blocks are not rigid for this mode of vibration (Figure 9f).

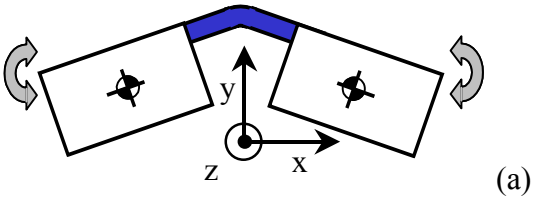

(a)

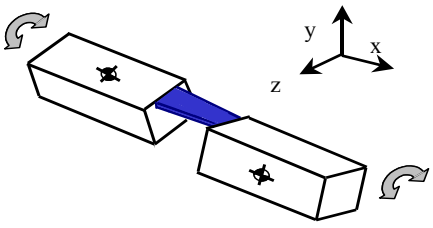

(b)

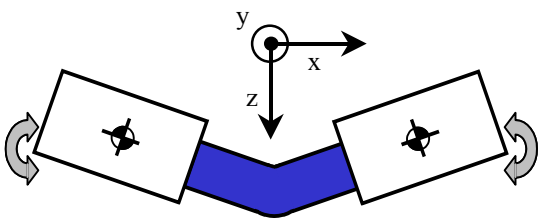

(c)

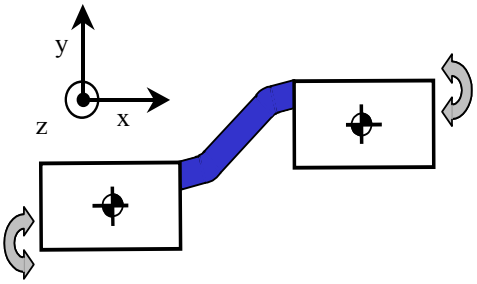

(d)

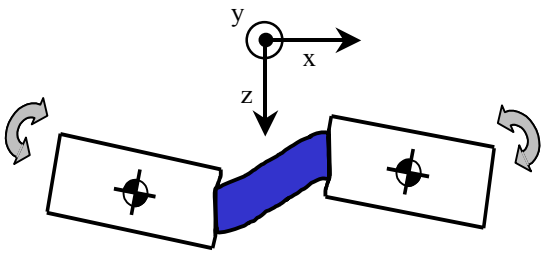

(e)

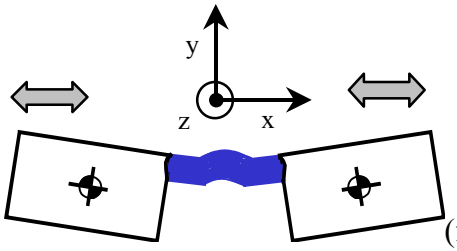

(f)

Figure 9. First six system mode shapes for Example D0. (a) Mode 1, rotation about z-axis. (b) Mode 2, twist about x-axis. (c) Mode 3, rotation about y-axis. (d) Mode 4, twist about z-axis. (e) Mode 5, twist about y-axis. (f) Mode 6, longitudinal displacement along x-axis. Refer to Figure 11a for typical dynamic compliance spectrum and Table 5 for associated natural frequencies.

In our study, the elastic joint (J) consists of two direct stiffness terms (rotation and shear) and two cross terms (due to coupling between rotational and shear stiffness). Moreover the blocks (A and B) are assumed to be rigid. Considering these constraints, the scope of the study covers only two modes with motion in the x-y plane. First, rotation of rigid blocks about the z-coordinate is re-designated as r = 1 mode. Second, out of phase rotation of two rigid blocks about the z-coordinate is re-classified as r = 2 mode. If only these two mode shapes needs to be included in the study, clearly assembly moves only in the x-y plane and hence only two DOFs are considered in this study. From henceforth, these modes are labeled with superscripts 1 and 2. Further, the frequency range of interest extends slightly beyond f^2.

Methods / Examples	Natural Frequencies (f_r)			Mode Shapes (Φ_r)			Modal Damping Ratios (ς_r)		
	EXP	FEM	SIM	EXP	FEM	SIM	EXP	FEM	SIM
C0-C8	--	✔	--	--	✔	--	--	--	--
D0	✔	✔	✔	--	✔	✔	✔	--	--
E0	--	✔	✔	--	✔	✔	--	--	--
E1-E5	✔	✔	--	--	✔	--	✔	--	--
F01-F02	✔	✔	✔	--	✔	✔	--	--	--
F1-F2	✔	--	--	--	--	--	✔	--	--

Table 4. List of modal properties available for Examples using three methods.

Example	Natural frequencies (Hz)											
	Measured (EXP)						Computed (FEM)					
	r =1	r =2	r =3	r =4	r =5	r =6	r =1	r =2	r =3	r =4	r =5	r =6
D0	115 ❶	290	486	607 ❷	2025	2795	113 ❶	283	478	594 ❷	1978	2748
E1	72 ❶	213	284 ❷	355	1767	2250	75 ❶	265	294 ❷	387	1576	1800
E2	70 ❶	227	258 ❷	298	1022	1993	69 ❶	234	262 ❷	269	900	1670
E3	105 ❶	263	372	532 ❷	1386	2500	110 ❶	268	302	564 ❷	1053	2246
E4	80 ❶	263	310 ❷	400	1466	1940	76 ❶	264	300 ❷	385	1421	1913
E5	115 ❶	290	467	638 ❷	1904	2745	115 ❶	288	447	635 ❷	1798	2626

Table 5. Comparison of natural frequencies for Examples D0 and E1-E5 with free-free boundary condition.
Key: ❶ First mode of interest; ❷ second mode of interest.

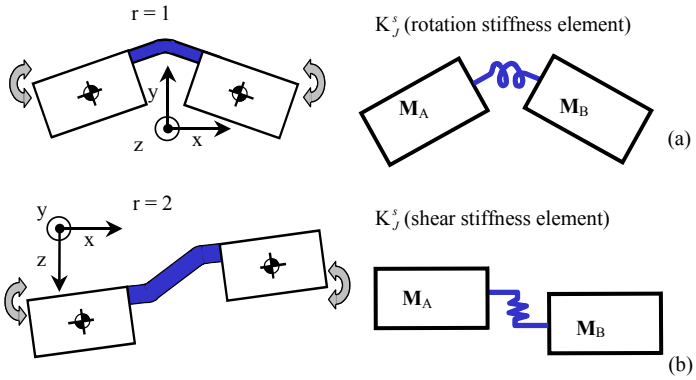

Figure 10. Representation of assembly's mode shape in terms of key joint stiffness elements. (a) Rotational stiffness element for r = 1 mode. (b) Shear stiffness element for r = 2 mode.

EXPERIMENTAL DATA

Measured dynamic compliance spectra ($\tilde{Y}_4/\tilde{F}_2$) of Example D0 and ($\tilde{Y}_4/\tilde{F}_1$) for Example E3 are shown in Figure 11a-b. In both plots, three peaks are clearly visible that are associated with r = 1 mode ($f_{r=1} = f^1$ Hz), r = 4 mode ($f_{r=4}$, = f^2 Hz) and r = 6 mode ($f_{r=6}$, Hz), in addition, peaks of smaller magnitudes can also be observed. It is found that frequencies associated with the latter correspond to mode r = 2 ($f_{r=2}$, Hz), r = 3 ($f_{r=3}$, Hz) and r = 5 ($f_{r=5}$, Hz). Refer to Figure 9 for associated mode shapes and Table 5 for natural frequencies. Figure 12a shows variations in $\tilde{Y}_4/\tilde{F}_1$ of Examples D0, E1, E2 and E3. Frequency shift in the peaks associated with f^1 and f^2 is clearly visible. Intuitively, one expects that natural frequencies (f_r) in all cases should be the same since the beam and blocks are unchanged. Nevertheless, it can be observed that f_r values for Examples E1 and E2 are quite lower than respective natural frequencies (f_r) of Examples D0 and E3. This indicates that the values of assembly stiffness matrix ($\tilde{\mathbf{K}}_j^d(\omega)$) in these four examples are different though the mass matrix (**M**) is the same. The only difference in these examples is the interfacial connection between the beam (E) and rigid blocks (A and B). Figure 12b shows variations in the dynamic compliance $\tilde{Y}_4/\tilde{F}_2$ between Examples D0, E4 and E5. Again, a similar trend in natural frequency shift is observed. One unexpected fact can be noticed in the Figure 12b. Now natural frequencies (f^1 and f^2) for Example E5 are higher than that of Example D0, integral (ideal) joint. Which indicates that interfacial connection in Example E5 (welded), is stiffer than Example D0 (integral). Also, lightly excited peaks associated with "not of interest" modes can be observed.

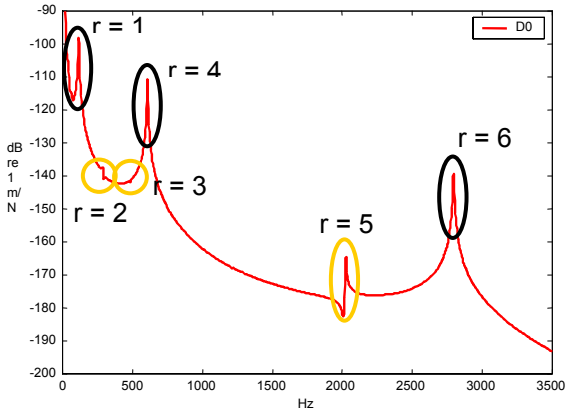

(a)

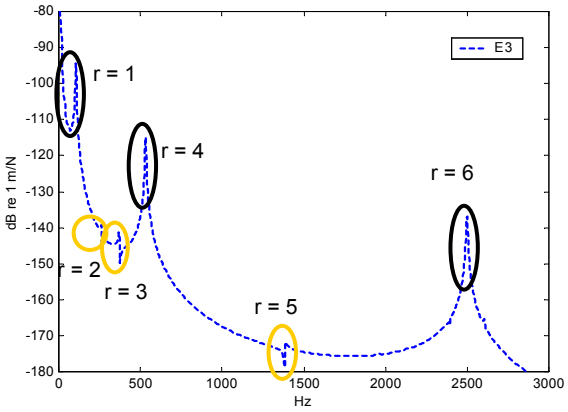

(b)

Figure 11. Measured dynamic compliance spectra. (a) Example D0. (b) Example E3. Key: ——— D0, – – – E3, ◯ mode of interest and ◯ mode not considered in this study.

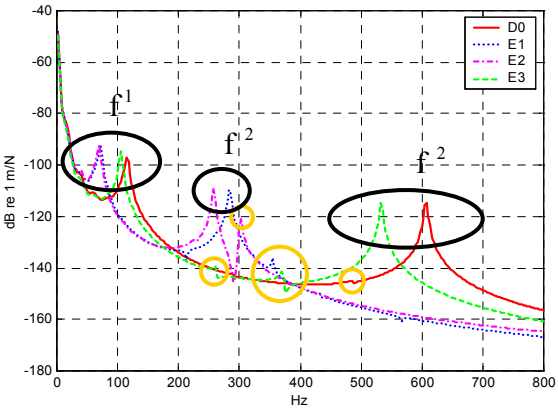

(a)

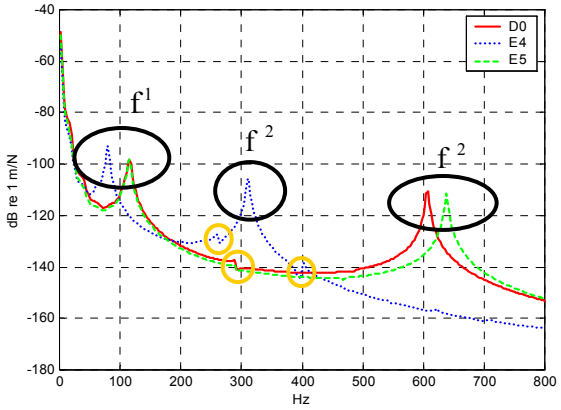

(b)

Figure 12. Comparison of dynamic compliance magnitudes. (a) $\tilde{Y}_4/\tilde{F}_1$ between Examples D0 and E1-E3. (b) Y_4/F_2 between Examples D0 and E4-E5. Key: D01, E1 (E4), E2, E3 (E5), mode of interest and mode not considered in this study.

Comparison between Examples F01 and F1 using accelerance $\tilde{Y}_4/\tilde{F}_1$ spectra is displayed in Figure 13a. As assembly in Example F1 is heavily damped, decreases in natural frequencies (f^1 and f^2), and magnitude levels are observed. Figure 13b compares $\tilde{Y}_4/\tilde{F}_1$ for Example F02 and F2. Here a variation in natural frequencies is less compared to Example F1. Also, some lightly excited peaks are observed that correspond to modes "not of interest". This reasoning is verified by comparing natural frequencies obtained from FEM models with experimental results as listed in Table 5. In columns three and four of measured (EXP) and computed (FEM) the natural frequencies (f_r) second mode of interest is observed. Specifically, for welded joint Examples E1, E2 and E4, modes three (r = 3) and four (r = 4) are interchanged that indicates that dynamic properties of system are sensitive to the configuration of joint.

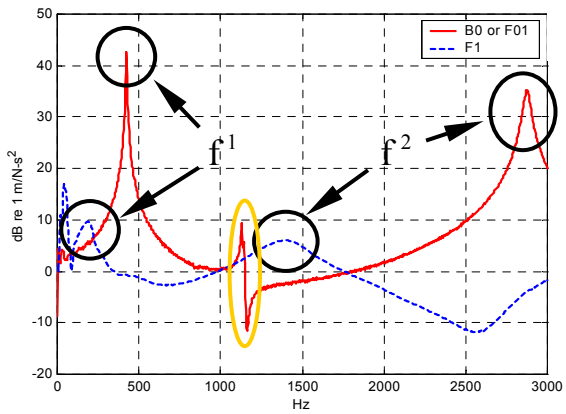

(a)

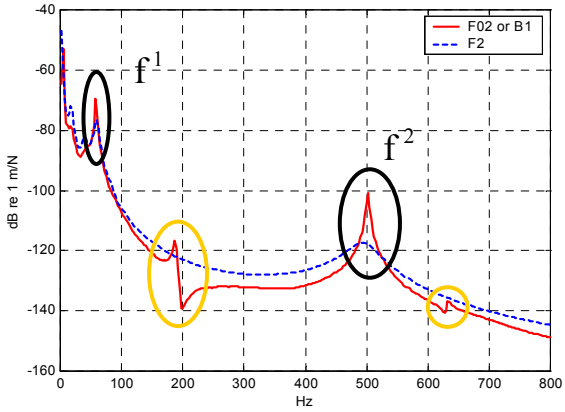

(b)

Figure 13. Comparison of FRFs for glued joints. (a) $\tilde{Y}_4/\tilde{F}_1$ between Examples F01 and F1. (b) $\tilde{Y}_4/\tilde{F}_1$ between Examples F02 and F2. Key: F01 (F02), F1 (F2), mode of interest and mode of not interest.

Before extracting modal damping ratios (ζ_r) associated with modes of interest, accuracy of experimental data is verified via coherence spectra. Coherence ranges from 0-1, 1 being perfect correlation between input and output signals. Figure 14a shows coherence of FRF $\tilde{Y}_4/\tilde{F}_1$ for Examples D0, E1, E2 and E5. Examples F1 and F2 are displayed in Figure 14b. Excellent coherences can be observed from the plots indicating experimental data with minimal random noise and LTI system. Modal damping ratios associated with modes of interest ($\zeta^1$and ζ^2) are obtained for Examples D0, E1-E5, F01, F02, F1 and F2. There are 8 FRFs for each example, associated with forces at locations 1 ($\tilde{F}_1(\omega)$) and 2 ($\tilde{F}_2(\omega)$). These 8 FRFs are used to obtain modal damping ratios (Table 6). As expected, damping ratios are very high for Examples F1 and F2 due to presence of glued (epoxy) interfaces.

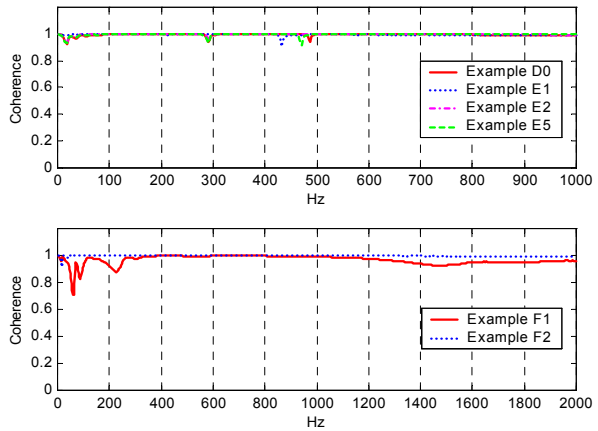

(a)

(b)

Figure 14. Comparison of coherence spectra for $\tilde{Y}_4/\tilde{F}_1$ (a) Examples D0, E1, E2 and E5. (b) Example F1 and F2. Key: D0 (F1), E1 (F2), E2 and E3.

Example	Modal Damping ratios ς_r (%)	
	r = 1 (ς^1)	r = 2 (ς^2)
D0	1.16	0.13
E1	0.92	0.28
E2	1.51	0.15
E3	0.26	0.11
E4	1.09	0.19
E5	1.30	0.08
F01	0.9	0.78
F02	2.9	0.50
F1	27.06	15.37
F2	2.44	4.14

Table 6. Measured damping ratios for Examples D0, E1-E5, F01, F02, F1 and F2.

Example	Natural Frequencies (Hz)					
	Calculated (SIM)		Measured (EXP)		Computed (FEM)	
	1	2	1	2	1	2
F01	532	4,019	423	2,872	434	2,900
F02	67	502	58	502	57	474
D0	148	723	115	607	117	612
E0	147	724	---	---	117	612

Table 7. Comparison of natural frequencies for integral joint examples (D and E0) with effective thickness values.

Example	Natural Frequencies of interest f^1 and f^2 (Hz)					
	Calculated using Analytical Lumped Model (SIM)		Measured (EXP)		Computed using Finite Element Model (FEM)	
D0	125	617	115	608	117	611
E0	126	618	---	---	117	612
E1	---	---	71	284	80	316
E2	---	---	70	258	70	266
E3	---	---	105	533	114	581
E4	---	---	79	311	77	299
E5	---	---	115	638	120	655
F01	420	3180	423	2872	434	2900
F02	67	502	58	502	57	474
F1	---	---	198	1414	---	---
F2	---	---	60	497	---	---

Table 8. Validation of natural frequencies for Examples D, E and F

Natural frequencies for Example C0 (Hz)		Example	Dimensional frequencies (Hz)		Dimensionless Frequencies (Hz)	
f^1	f^2		f^1	f^2	$\overline{f_{C0}^1}$	$\overline{f_{C0}^2}$
316	3234	C1	127	270	0.40	0.08
		C2	57	93	0.18	0.03
		C3	142	356	0.44	0.11
		C4	179	685	0.57	0.21
		C5	283	2545	0.90	0.78
		C6	282	2500	0.89	0.77
		C7	280	2475	0.88	0.77
		C8	282	2508	0.89	0.78

Table 9. Dimensional and non-dimensional natural frequencies for Example C.

As now, natural frequencies ($f^1$and f^2) and mode shapes from EXP and FEM models with two DOFs are available, SIM model for Examples D0, E0, F01 and F02 is verified (Table 7). Notice that for SIM model of Example D0, E0 and F01, natural frequencies (f^1 and f^2) are high compared to EXP and FEM models. This variation may be due to the fact that a beam with aspect ratio less than 20 cannot be modeled by the Euler beam theory [11]. The beam aspect ratio for Example F01 is 5.2, 21 for Example F02 and 12 for Examples D0 and E0. The aspect ratio for Example F02 is greater than 20 and thus SIM results are in good agreement with EXP and FEM models. This issue is resolved by taking an effective thickness of the elastic beam. Beam thickness is reduced by 15% for Example F01, 10% for Examples D0 and E0 to bring the SIM results within 10% range of EXP and FEM results. Natural frequencies (f^1 and f^2) calculated using effective beam thickness, are compared with EXP and FEM results in Table 8.

EFFECT OF WELD CONFIGURATION

Example C0 is an integral joint, also called as the ideal joint. Examples C1 through C8 represents theoretical FEM models with different weld configurations of Figure 3. In all examples, nodal DOFs are constrained such that assembly can translate only along the y-axis and rotate about the z-axis. Natural frequencies and mode shapes are obtained. When non-dimensional frequencies are plotted an "S" curve (Figure 15) is observed. Here, $\overline{f_{C0}^1}$ and $\overline{f_{C0}^2}$ are the dimensionless first and second natural frequencies of an assembly for Examples C1-C8 (Table 9). In order to find dimensionless natural frequencies, the natural frequencies of Example C0 are used as the reference. Values close to unity in the non-dimensional natural frequency indicate weld configuration has stiffness similar to that of the integral (ideal) joint and a value closer to 0 indicates that the weld configuration is very compliant. Two key points should be noticed here: natural frequencies (f^1 and f^2) for Examples C5-C8 are almost the same and there is a transition zone between natural frequencies (f^1 and f^2) of Examples C4 and C5. This transition indicates how a weld configuration can influence the dynamic property of an assembly. The natural frequency has greatest sensitivity to a specific joint stiffness value as related to weld configuration in the middle part of this 'S' curve. Similar trend is reported by Singh et. al., for plate structures joined with different types of joints [1].

FEM MODELING ISSUES FOR EXAMPLE E

The weld joining rigid blocks (A and B) and elastic beam (E) is considered as a lump of steel. In creating simplified FEM models, weld is modeled using simple geometric shapes such as rectangles and triangles, as shown in Table 3. Given the available structures (Examples E1-E5), dimensions of such simple shapes are assumed, and weld configurations were selected by trial and error such that natural frequencies of interest (f^1 and f^2) remain in good agreement with measured (EXP) data. In Example E2, the weld joint was modeled as shown in Figure 16. It is assumed that in addition to weld on the upper edge of the interface (block $\ell_w \times w_w \times h_w(1)$), some amount of weld is between the rigid block (A or B) and beam (E), below the upper edge (block $\ell_w \times w_w \times h_w(2)$). Variations in the weld dimensions vary natural frequencies (f^1 and f^2) of an assembly varies drastically. For the sake of illustration, natural frequencies are obtained by varying $h_w(2)$ from 0 mm to 2.00 mm while holding all other dimensions (Table 10). Notice when $h_w(2)$ = 0 mm, natural frequencies of the system are 50% lower than that obtained from measured data. With an increase in the value of $h_w(2)$, natural frequency rises. Similar approach is adopted to model all other FEM models of Examples E1-E5, refer to Table 3 for weld dimensions. Natural frequencies obtained using FEM and EXP models for Examples E1-E5 are displayed in Figure 17. FEM predictions are within 10 % range of measured results.

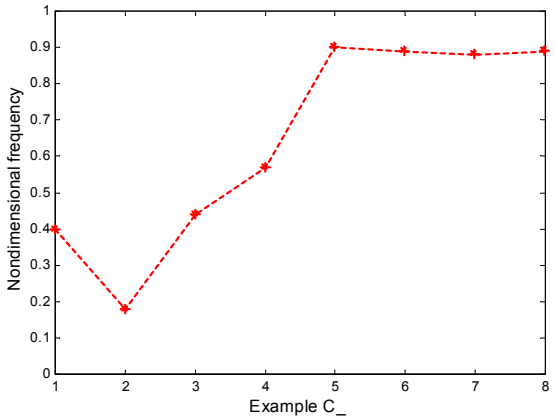

Figure 15. Non-dimensional frequency ratios for cases C1-C8. (a) $\overline{f_{C0}^1}$ (b) $\overline{f_{C0}^2}$.

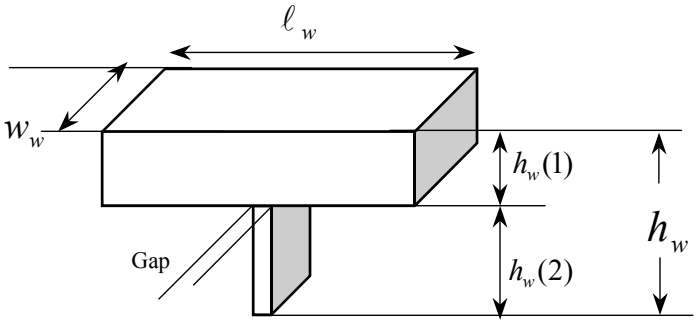

Figure 16. Magnified view of the weld used in FEM model for Example E2.

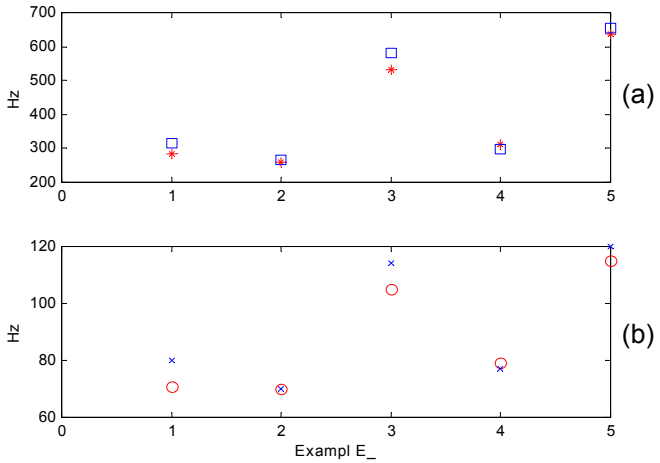

Figure 17. Comparison of natural frequencies for Examples E1-E5. (a) Second natural frequency. (b) First natural frequency. Key: * 2nd Exp, □ 2nd FEM, O 1st EXP, X 1st FEM.

Weld dimensions (mm) (Figure 16)		Predicted natural frequencies (Hz)	
Other dimensions	$h_w(2)$	f 1	f 2
		70 (EXP)	258 (EXP)
$\ell_w = 5.1$ $w_w = 15$ $h_w(1) = 3$ Gap = 0.1	0.00	30	102
	0.50	42	149
	1.00	53	192
	1.25	58	211
	1.50	63	233
	2.00	72	274

Table 10. Natural frequencies predicted by FEM models for E2 given different weld heights.

CONCLUSION

Examination of mode shapes shows that only two modes are within the frequency range of interest. First and second modes of interest have planer motions in the x-y plane and represent rotational and shear stiffness elements of joint respectively. Modal analysis of the lumped mass analytical model (SIM) with effective beam dimensions for the integral joint examples (D0, E0, F01 and F02) yield natural frequencies that are within 10% of measured data. Appropriate geometrical dimensions of welded joints in finite element models (Examples E1-E5) must be judiciously selected. Again, natural frequencies and mode shapes computed are within 10% of experimental data. Measured FRFs of welded examples show a variation in natural frequencies from 70 to 115 Hz for the first mode and from 284 to 638 Hz for the second mode. This clearly suggests the importance of properly modeling joints and quantifying their stiffnesses. Therefore techniques are needed to extract stiffness and damping matrices of joints. It is discussed in the companion paper [12].

ACKNOWLEDGEMENT

We are grateful to the Edison Welding Institute (EWI) and the Center for Automotive Research (CAR) Consortium for financially supporting this research. Special thanks go to Dr. Jeff Cropmton of EWI for his suggestions and help in fabricating welded fixtures. We would like to also thank Dr. Mayank Tiwari and Matt Young for their work during the earlier phase of the project.

REFERENCES

1. R. Singh, M.L. Liaw, J.E. Farstad and S.W. Kung, Determination of Joint Stiffness through Vibration Analysis of Beam Assemblies, Edison Welding Institute Research Report, MR9502, 1995.
2. Y. Ren and C.F. Beards, On the Nature of FRF Joint Identification Technique, Proceedings of the 11th International Modal Analysis Conference, V.1 (of 2) pp. 473-478, 1993.
3. M. Kamal and J. Wolf, Modern Automotive Structure Analysis, Van Norstrand Reinhold Company, 1982.
4. M. Young, Identification of joint Stiffnesses Using a Component Synthesis Technique, M.S. Thesis, The Ohio State University, 2000.
5. ANSYS Inc <www.ansys.com>.
6. R. Singh, The Ohio State University, ME 778 Course Notes, pp. 44-88, 228-286, 2000.
7. D.J. Ewins, Modal Testing: Theory and Practice, Research Studies Press, 1984.
8. LMS International <www.lmsintl.com>.
9. W.T. Thomson and M.D. Dahleh, Theory of Vibration with Applications, Prentice Hall, 4th ed., pp.172-173, 292-293, 1998.
10. The Mathworks <www.mathworks.com>
11. A.W. Leissa, The Ohio State University ME 734 Course Notes, pp. 4.1-4.54, 2000.
12. P. Mehta and R. Singh, Estimation of Dynamic Stiffness Matrix of Welded or Glued Joints Using a Laboratory Fixture, SAE Paper # 03NVC-252.